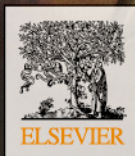


ISSN 2095-9273  
CN 10-1298/N  
科学通报 (英文版)

# Science Bulletin

Volume 63 · Number 4 · February 2018



 SCIENCE CHINA PRESS

Chinese Academy of Sciences  
National Natural Science Foundation of China



## Article

# A flattened enantiornithine in mid-Cretaceous Burmese amber: morphology and preservation

Lida Xing<sup>a,b,1</sup>, Jingmai K. O'Connor<sup>c,1</sup>, Ryan C. McKellar<sup>d,e,f,\*,1</sup>, Luis M. Chiappe<sup>g</sup>, Ming Bai<sup>h,1</sup>, Kuowei Tseng<sup>i</sup>, Jie Zhang<sup>j</sup>, Haidong Yang<sup>h</sup>, Jun Fang<sup>b</sup>, Gang Li<sup>j,\*,1</sup>

<sup>a</sup>State Key Laboratory of Biogeology and Environmental Geology, China University of Geosciences, Beijing 100083, China

<sup>b</sup>School of the Earth Sciences and Resources, China University of Geosciences, Beijing 100083, China

<sup>c</sup>Key Laboratory of Vertebrate Evolution and Human Origins of the Chinese Academy of Sciences, Institute of Vertebrate Paleontology and Paleoanthropology, Beijing 100044, China

<sup>d</sup>Royal Saskatchewan Museum, Regina, Saskatchewan S4P 4W7, Canada

<sup>e</sup>Biology Department, University of Regina, Regina, Saskatchewan S4S 0A2, Canada

<sup>f</sup>Department of Ecology and Evolutionary Biology, University of Kansas, Lawrence 66045, USA

<sup>g</sup>Dinosaur Institute, Natural History Museum of Los Angeles County, Los Angeles 90007, USA

<sup>h</sup>Key Laboratory of Zoological Systematics and Evolution, Institute of Zoology, Chinese Academy of Sciences, Beijing 100101, China

<sup>i</sup>Department of Exercise and Health Science, University of Taipei, Taipei 11153, China

<sup>j</sup>Institute of High Energy Physics, Chinese Academy of Sciences, Beijing 100049, China

## ARTICLE INFO

## Article history:

Received 11 September 2017

Received in revised form 2 January 2018

Accepted 3 January 2018

Available online 31 January 2018

## Keywords:

Enantiornithes

Juvenile

Osteology

Soft tissue preservation

## ABSTRACT

Cretaceous amber from Myanmar (~99 Ma Burmese amber) has become a valuable supplement to the traditional skeletal record of small theropod dinosaurs preserved in sedimentary rocks, particularly for coelurosaurs and enantiornithines. The specimens recovered from this deposit preserve skeletal material and soft tissues in unmatched detail. This provides opportunities to study three-dimensional preservation of soft tissues, microstructure, and pigmentation patterns that are seldom available elsewhere in the fossil record. Ultimately, this line of research provides insights into life stages that are difficult to preserve, the ecology and appearance of the groups involved, and the evolutionary-development of structures such as feathers. Here we describe the most recent discovery from Burmese amber, an articulated skeleton of an enantiornithine bird. This individual has been sectioned along the coronal plane, providing a unique view inside multiple body regions. Osteological observations and plumage patterns support placement within the Enantiornithes, and suggest that the animal may have been a juvenile at the time of death. The specimen has a complex taphonomic history that includes exposure at the surface of a resin flow prior to encapsulation, and may include scavenging by some of the insects trapped within the same amber piece. The chemical composition observed along surface exposures and shallowly buried regions of the body indicate that the specimen has not undergone significant exchange with its surroundings. High iron concentrations are present in regions that preserve soft tissues as carbon films, and calcium distribution corresponds to regions where bones breach the surface of the amber.

© 2018 Science China Press. Published by Elsevier B.V. and Science China Press. All rights reserved.

## 1. Introduction

Recent discoveries of mid-Cretaceous amber from Myanmar (reviewed by [1–3]) have provided unprecedented information for understanding the early post-natal development of early birds. Over the last two years, Xing et al. [4–6] have described two

precocial Enantiornithes wings and a partial hatchling, as well as a feathered coelurosaurian tail with primitive plumage from mid-Cretaceous Burmese amber. These new findings associate well-preserved feathers with skeletal material for the first time. They also highlight the unique preservation potential of amber for understanding the morphology and evolution of vertebrate integumentary structures. However, despite these advances, findings over the last two years have largely been limited to partial or appendicular skeletal material, due to the small sizes of the amber pieces involved.

\* Corresponding authors.

E-mail addresses: [ryan.mckellar@gov.sk.ca](mailto:ryan.mckellar@gov.sk.ca) (R.C. McKellar), [lig@ihep.ac.cn](mailto:lig@ihep.ac.cn) (G. Li).

<sup>1</sup> These authors contributed equally to this work.

To date, enantiornithines remains in amber consist of one isolated wing tip (DIP (Dexu Institute of Palaeontology, Chaozhou City, China)-V-15101), that may have been disassociated from the corpse through decay or predation; one wing tip (DIP-V-15100) that appears to have been part of a much more complete skeleton, which was destroyed during the mining process or subsequent polishing of the surrounding amber in preparation for jewelry manufacture [4]; and a partial hatchling (HPG (Hupoge Amber Museum, Tengchong City Amber Association, China)-15-1) that included most of the skull, part of the neck, one wing, and both feet [6]. The size bias that is prevalent in the amber fossil record [7] has meant that most of the finds in Burmese amber have belonged to small, precocial juveniles the size of modern hummingbirds. These specimens have supplemented our understanding of Enantiornithes compression fossils with comparatively limited soft tissue preservation in Cretaceous rocks from Argentina [8], Brazil [9], China [10–12] Mongolia [13], Spain [14,15], and the USA [16].

Preservation among the Burmese amber skeletal specimens has been variable, depending on the size of the specimen and the degree to which the remains have been exposed to weathering, decay, and compaction prior to full resin polymerization. In the best-preserved specimens, bones are found in articulation and without significant deformation or replacement (e.g., DIP-V-15100, where intact osteon structures are visible; [4]). However, deformation of the surrounding resin mass has shattered, scattered, or compressed the thin and hollow bones of some specimens (e.g., HPG-15-1, where the metatarsals and digits are encapsulated in soft tissue, but the bones are fragmentary; [6]). Where bones have been exposed at the amber surface, providing a conduit for pore waters, some specimens exhibit infilling or partial replacement of bones by clay minerals (e.g., DIP-V-15103, where bone replacement limits X-ray  $\mu$ CT scanning contrast; [5]).

The areas available for chemically examining preservation within the amber have been limited by the available surface exposures, but SR  $\mu$ XFI (synchrotron radiation micro-X-ray fluorescence imaging) and XAS (X-ray absorption spectroscopy) have proven valuable as non-destructive tools for mapping the chemistry and probing the oxidation state of individual elements within these amber specimens [5]. In combination, these techniques have shed additional light on the preservation process for vertebrate inclusions within Burmese amber, permitting comparisons to discoveries in sedimentary rocks (e.g., [16–18]).

Here we describe the contents of the largest piece of Burmese amber with theropod inclusions known to date: an enantiornithine including much more of the axial skeleton. This specimen allows us to examine preservational processes in greater detail, providing the first internal view of multiple body regions in one of these inclusions, and an expansive surface for chemical mapping.

## 2. Materials and methods

### 2.1. Specimen and photography

The new amber specimen, DIP-V-15102, comes from the Angbamo site, Tanai Township (Myitkyina District, Kachin Province) of northern Myanmar. It measures approximately 68 mm  $\times$  7 mm  $\times$  51 mm, and weights 14.99 g. The original specimen is housed and displayed in the Dexu Institute of Palaeontology (=DIP), China.

DIP-V-15102 was examined using a Leica MZ 12.5 stereomicroscope with a drawing tube attachment. Photographs were taken

using a Canon digital camera (5D Mark III, MP-E 65MM F/2.8 1–5X) fitted to a macro rail (Cognisys), and were processed using Helicon Focus 5.1 and Adobe Photoshop CS5 software to increase depth of field in the images. These images were supplemented with photos taken under long wavelength UV light (395 nm), mapping resin flows.

### 2.2. Micro-CT scanning and 3D reconstruction

DIP-V-15102 was scanned with a MicroXCT 400 (Carl Zeiss X-ray Microscopy, Inc., Pleasanton, USA) at the Institute of Zoology, Chinese Academy of Sciences. The scans of the entire animal were completed by dividing the specimen into seven scans that were done with a beam strength of 60 kV, 8 W, absorption contrast and a spatial resolution of 43.3249  $\mu$ m. The different parts of the bird (head, hip, apical forelimb, radius-ulna area, dorsal vertebrae) were scanned separately in higher resolution, with a beam strength of 60 kV, 8 W, absorption contrast and the spatial resolution of 19.4520  $\mu$ m, 20.9483  $\mu$ m, 20.9483  $\mu$ m, 4.2520  $\mu$ m, 4.2520  $\mu$ m, respectively.

Based on the image stacks obtained, structures of the specimen were reconstructed and separated with Amira 5.4 (Visage Imaging, San Diego, USA). The subsequent volume rendering and animation were performed with VG Studiomax 2.1 (Volume Graphics, Heidelberg, Germany). Final figures were prepared with Photoshop CS5 (Adobe, San Jose, USA) and Illustrator CS5 (Adobe, San Jose, USA).

### 2.3. $\mu$ -XFI chemical mapping

The  $\mu$ -XFI analysis was performed at 4W1B beamline, Beijing Synchrotron Radiation Facility, which runs 2.5 GeV with a current of 250 mA in SR-dedicated mode. The incident X-ray is monochromatized by the W/B4C Double Multilayer Monochromator at 15 keV and is focused down to 100  $\mu$ m in diameter by a polycapillary lens. The two-dimensional mapping is acquired in step-mode: the sample is held on a precision motor-driven stage, scanning 100  $\mu$ m stepwise. The Si(Li) solid state detector is used to detect X-ray fluorescence emission lines with an exposure time of 20 s. Data reduction and processing were performed using the PyMca software package [19]. Herein, the feather and skin terminology presented by Lucas and Stettenheim [20] is largely followed, while details related to barbule morphology and pigmentation follow Dove [20].

## 3. Results

### 3.1. Osteological characters

DIP-V-15102 is an articulated skeleton (Fig. 1). The dense feathers and their well-developed rachises suggest this specimen represents a bird. Most avian records in Burmese amber consist of isolated feathers or partial bones. Consequently, the discovery of an articulated skeleton is an extremely rare event. DIP-V-15102 was cut and polished by a local miner along the coronal plane prior to study, losing the rostral and middle portions of the skull and most of its right wing and leg. However, the surviving skeletal portions still render the specimen the most complete individual discovered thus far in Burmese amber.

Remains of the right basicranium (part of the frontal and parietal region), axial column (about 5 cervical vertebrae and 8 dorsal vertebrae), forelimb (distal right humerus, radius and ulna), partial pelvic girdle and right femur are preserved in articulation (Fig. 1c, d). All bones are very compressed and the degree of co-fusion

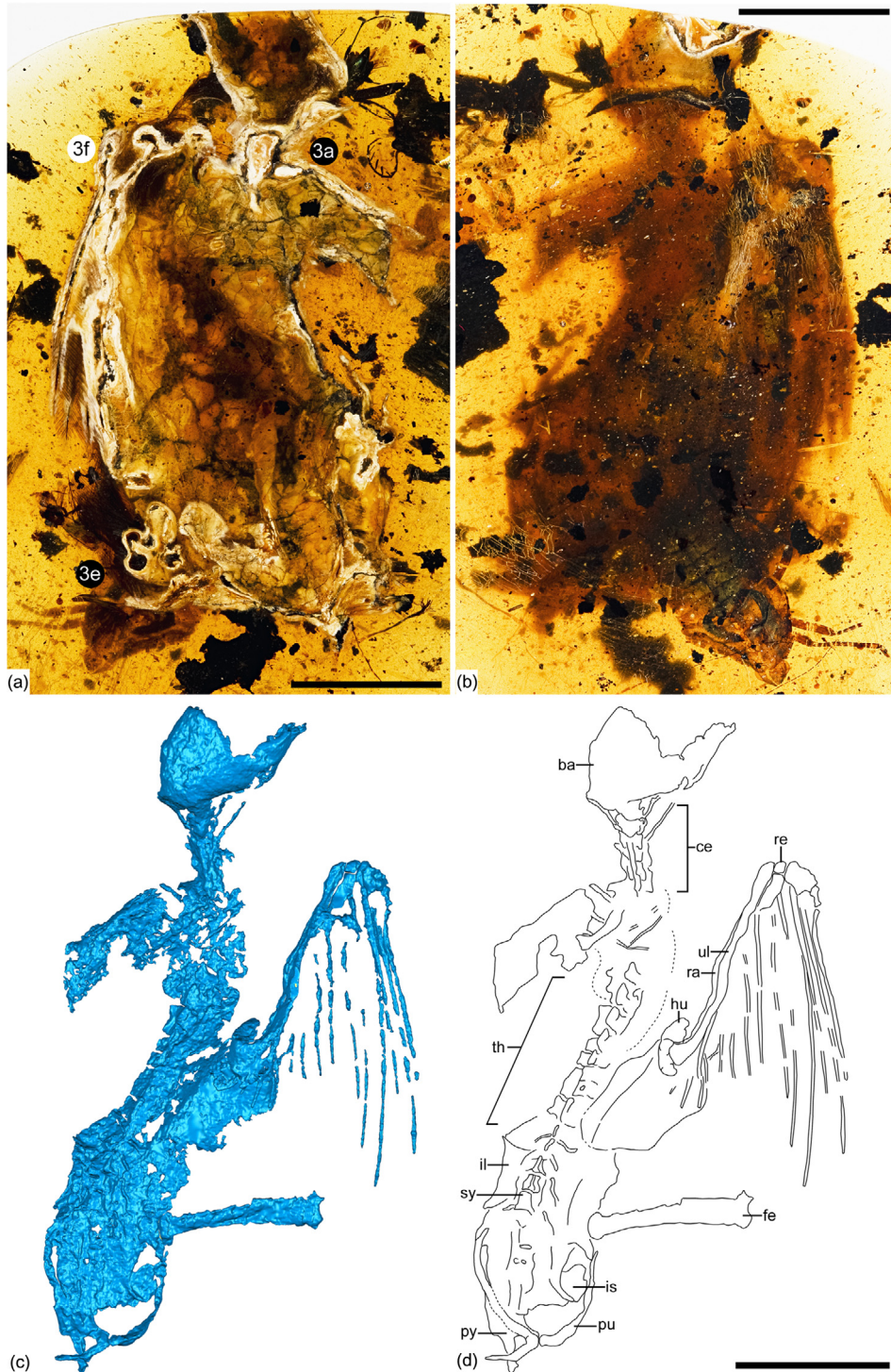


**Fig. 1.** DIP-V-15102 specimen overview and corresponding X-ray  $\mu$ CT renderings. (a) Ventrolateral view of coronal section through body, with reference points for more detailed images in Fig. 2; (b) Dorsolateral surface of body with skull breaching amber surface along upper edge of amber piece, and cockroach syninclusion visible near lower margin of image; (c) Composite rendering of preserved bones and soft tissue in dorsolateral view; (d) Outlines of identifiable bones and soft tissues present in scan data. Scale bars equal 10 mm. Abbreviations: ba, basicranium; ce, cervical vertebrae; fe, femur; il, ilium; is, ischium; hu, humerus; pu, pubis; py, pygostyle; ra, radius; re, radiale; sy, synsacrum; th, thoracic vertebrae; ul, ulna.

between elements is obscured by the quality of the scan. The cervical vertebrae preserve no clear anatomical information. The thoracic series consists of nine to ten vertebrae in articulation, displaying large square-shaped neural spines. The sacral vertebrae

can be somewhat distinguished suggesting that fusion of the synsacrum was incomplete. A few free caudal vertebrae can be discerned. They appear to be followed by a robust triangular element interpreted as the pygostyle. The pubes are U-shaped,

strongly concave medially, with a short distal symphysis, as in enantiornithines. The distal right humerus is preserved; it appears to be dorsoventrally expanded, lacking any evidence of sulci tricipitalis, conditions present among many enantiornithines. The ulna is proximally bowed and more robust than the radius, as in other birds. A single rectangular carpal is preserved between the radius and the carpometacarpus; this bone is identified as the radiale. Only the proximal end of the carpometacarpus is preserved revealing the semilunate carpal trochlea. The alular metacarpal and potentially the first alular phalanx may also be preserved but this cannot be determined unequivocally from the scan data. The right

femur is missing the distal end and its articulation with the pelvis obscures the morphology of the proximal end.

### 3.2. Preservation

DIP-V-15102 provides many challenges due to its preservational state, but it also provides a unique internal view and good constraints on its taphonomic history. The specimen was accidentally cut at the coronal plane, giving us the opportunity to look inside the bird specimen and see a detailed sectional view of preservation in a larger vertebrate inclusion (Fig. 2). In the exposed

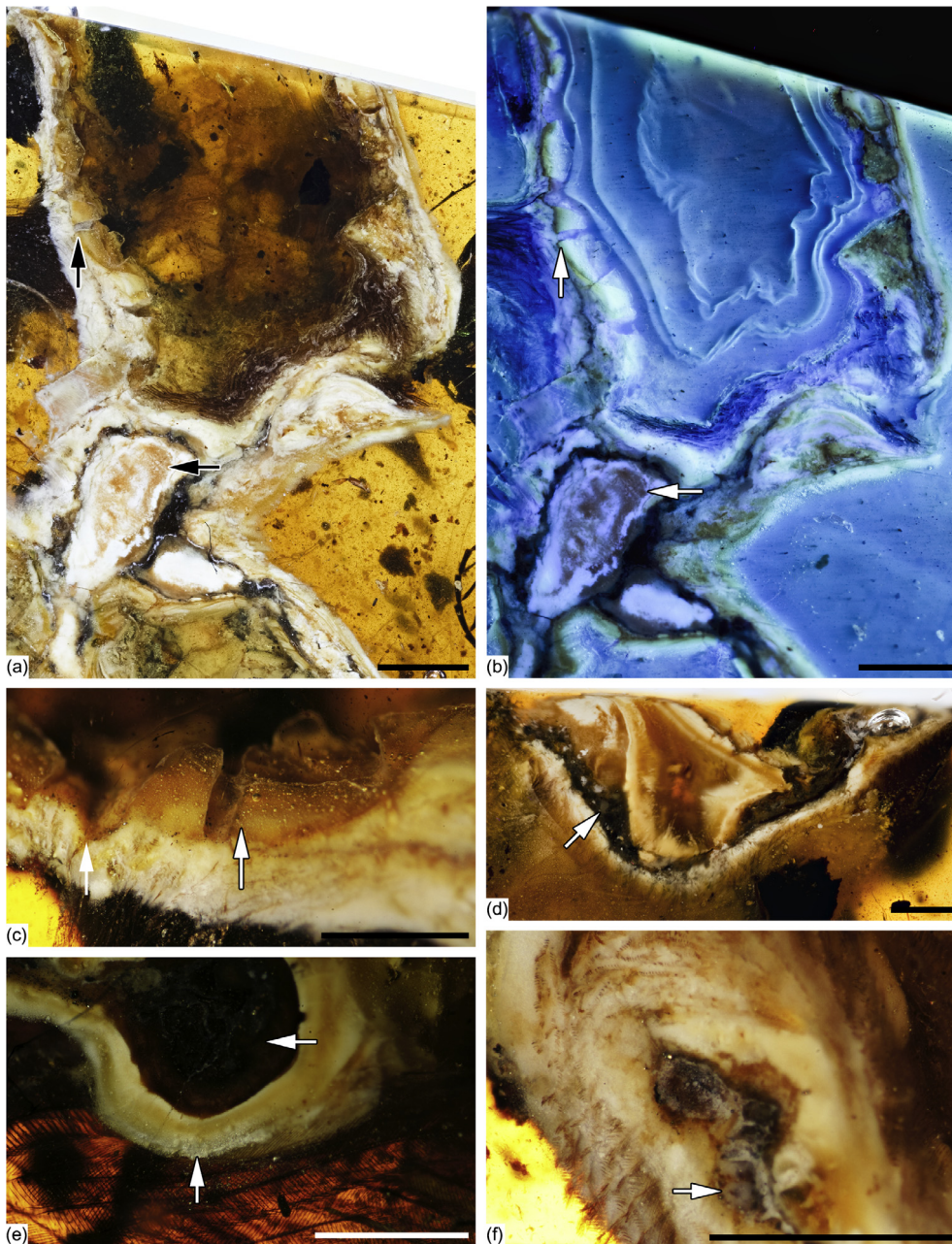


**Fig. 2.** Preservation of head, neck, and limb bones in DIP-V-15102. (a) Overview of head and neck region along coronal section, with vertical arrow indicating skull shards, and horizontal arrow indicating exposed cervical vertebrae; (b) UV light image corresponding to (a), showing concentric flow lines within cranial cavity, and dark regions of soft tissue and plumage preservation; (c) Detail of skull preservation in (a) and (b), with bone fragment (left arrow) and surrounded by fissures within milky amber veil (right arrow); (d) Dorsolateral exposure of skull, with sediment layer inside (arrow); (e) Cross-section of right femur, with indistinct exterior surface (vertical arrow), and organic rich infilling of the medullary cavity (horizontal arrow); (f) Cross-section of right wing bones (arrow) obscured by extensive veil of milky amber through which covert feathers protrude. Scale bars equal 2 mm (a, b); 1 mm (c–f).

areas, bones are visible as translucent masses that are rimmed by a dark carbon film (where soft tissues once existed). This, in turn, is surrounded by a pervasive and thick layer of ‘milky’ amber through which the feathers protrude. The nearly opaque milky layer makes it extremely difficult to gather surface observations of the bones, soft tissues, or integumentary structures, but it does shed some light on the preservational process.

The veil of milky amber appears to be a product of either moisture or decay products from the corpse interacting with the surrounding amber, creating a dense film of microscopic bubbles that render the amber nearly opaque. This is a common preservational feature in both Burmese and Baltic amber inclusions [4–7,22]. In DIP-V-15102, it is unclear how much of the opaque layer can be attributed to milky amber, as opposed to saponified tissues, because there is no distinct boundary between the skin surface and the surrounding amber. The inner surface of the body cavity has a much thicker veil than the outer (predominantly dorsal) surface, except adjacent to the head (Figs. 1a; 2a, c, f; S1): resin appears to have encountered more moisture or decaying material in these regions. However, there are no traces of the internal organs present in either the abdominal or cranial cavities. This, coupled with the deeply cracked surface of the milky veil inside the body cavity (Fig. 2a, c), and the apparent lack of soft tissues around the exposed femur (Figs. 2e; S3a, b), suggest that the ventral surface of the body and abdominal contents were weathered away before the body cavity was infilled by subsequent resin flows. Unlike the bones of one previously studied enantiornithine wing fragment (DIP-V-15100 [4]), or the coelurosaur tail fragment recovered from this deposit (DIP-V-15103 [5]), the new avialan does not show any strong signs of bone replacement or voids being infilled with clay minerals. The hollow shaft of the femur in DIP-V-15102 appears to be filled with dark, organic-rich material (Figs. 2e; S3a, b) that better matches the carbon films preserved in the areas originally containing soft tissues. However, cortical bone and the medullary cavity are less distinct in the regions where the manus breaches the surface of the amber (Fig. 2f).

The cranial cavity displays a concentric banding within its internal resin flows (Fig. 2b) and a thin layer of sediment along the posterodorsal margin (Fig. 2d), indicating infill by a series of flows that proceeded from dorsal to ventral while the skull was largely intact. While the resin still retained some plasticity, the body must have experienced significant deformation, because the bones of the skull are broken up into widely spaced shards (Fig. 2a–c), and the milky amber veil has corresponding fissures. Many postcranial bones are compressed but remain articulated or nearly so. The entire right wing has detached and drifted posteriad, situated near the mid-length of the thorax (Fig. 1b–d). The wing position suggests that this part of the body drifted away from the axial skeleton, either as a result of soft tissue decay and drifting before the resin began to polymerize, or after polymerization had already begun (as part of the same event that compacted the skull).

### 3.3. Integumentary structures

The right wing has 14–15 distinct rachises that are preserved well enough to show up in the X-ray  $\mu$ CT scan data (Fig. 1), representing 10 or 11 of the secondary flight feathers, and 4 of the basal primaries. (The distal primaries have been destroyed along the coronal section line.) Much of the plumage in DIP-V-15102 is obscured by overlying milky amber combined with a thick layer of amber clouded by organic particles (dorsally), but a few body regions are open to detailed observation through exposures near the surface.

Feathers are exposed along the coronal section for regions of the head, neck, and right wing. The posterior margin of the head bears a dense coat of short, loosely vaned contour feathers. Barbs among these feathers become broader and more elongate toward the base of the neck. These feathers have blade-like barbules that appear undifferentiated, but observations are biased toward barb apices—regions that typically bear reduced barbules in modern birds [20,21]. The barbule apices among the head feathers are preserved with a diffuse, dark brown pigmentation, while the barbule bases and barb rami appear to have been pale or unpigmented (Fig. 3a).

A mass of detached feathers is visible between the head and the wrist of the right wing. These feathers presumably stem from the shoulder or breast regions, since they include a mixture of contour feathers (similar to those found on the neck), and numerous semiplumes (Fig. 3b). The semiplumes have elongate, plumulaceous barbules without curvature or blade-like basal cells, but it is not possible to observe nodes and internodes among these barbules. Pigmentation among the semiplumes is uniform across all feather regions, appearing pale brown and diffuse.

Primary feathers among the wing plumage have deep rachises and rami that taper out into fine lines where they are cut obliquely by the sectional plane (Fig. 3c, e). Barbs among these feathers have strongly asymmetrical barbules that are narrow and separated from one another by a distance greater than the width of each barbule (Fig. 3e, f). Proximal barbules are relatively straight, diverging away from the rachis at approximately 50°, and gently curving apically. Distal barbules have strongly elbowed barbules that diverge from the ramus at approximately 70°, but angle apically at the base of a well-developed flagellum. The flagellum has expanded nodes, and few hooklets are visible among the apical barbules (Fig. 3g). Barbules, rami, and rachises are all diffuse, pale brown in colour; but pigmentation is slightly darker along the proximal edge of each barbule, and within its flagellum. Secondary remiges cannot be clearly identified or differentiated from the primaries in the surface views available; however, the feather apices that are exposed adjacent to the right femur may belong to this feather category, and these match the primaries in terms of visible pigmentation (Fig. 2e). The leading edge of the wing provides some small glimpses of major coverts protruding from the milky veil covering the wrist area, but only the apices of some barbs are visible here (Fig. 2f). These feathers may have more of a reddish-brown apparent coloration, and the barbs exhibit pale or unpigmented cores. The underside of the wing has a single small patch of covert feathers preserved near the wrist. Where microstructure is visible, these feathers are generally similar to the flight feathers, but have slightly narrower barbs containing a more narrowly spaced set of blade-shaped and smooth barbules. These coverts have more even pigment distribution than in the leading edge of the wing, but the nodes are paler, providing a clearer definition of the barbule subdivisions (Fig. 3h). Pigmentation outlines approximately 7 basal cells, followed by a narrow pennulum with 12 or more internodes. The underwing coverts appear to be overlapped by a few adjacent contour feathers from the body that have loose, flexible barbules with narrow and elongate shapes. Although these barbs share the same pale cores as the head plumage, the apical part of each barbule appears to be slightly darker in color.

### 3.4. $\mu$ -XFI results

The micro-X-ray fluorescence imaging ( $\mu$ -XFI) scanned region, includes the base of the skull, cervical vertebrae, and partial scapula area of the fossil. This region includes four subdomains marked in Fig. 4. Subdomain 1 corresponds to the inclusion, where

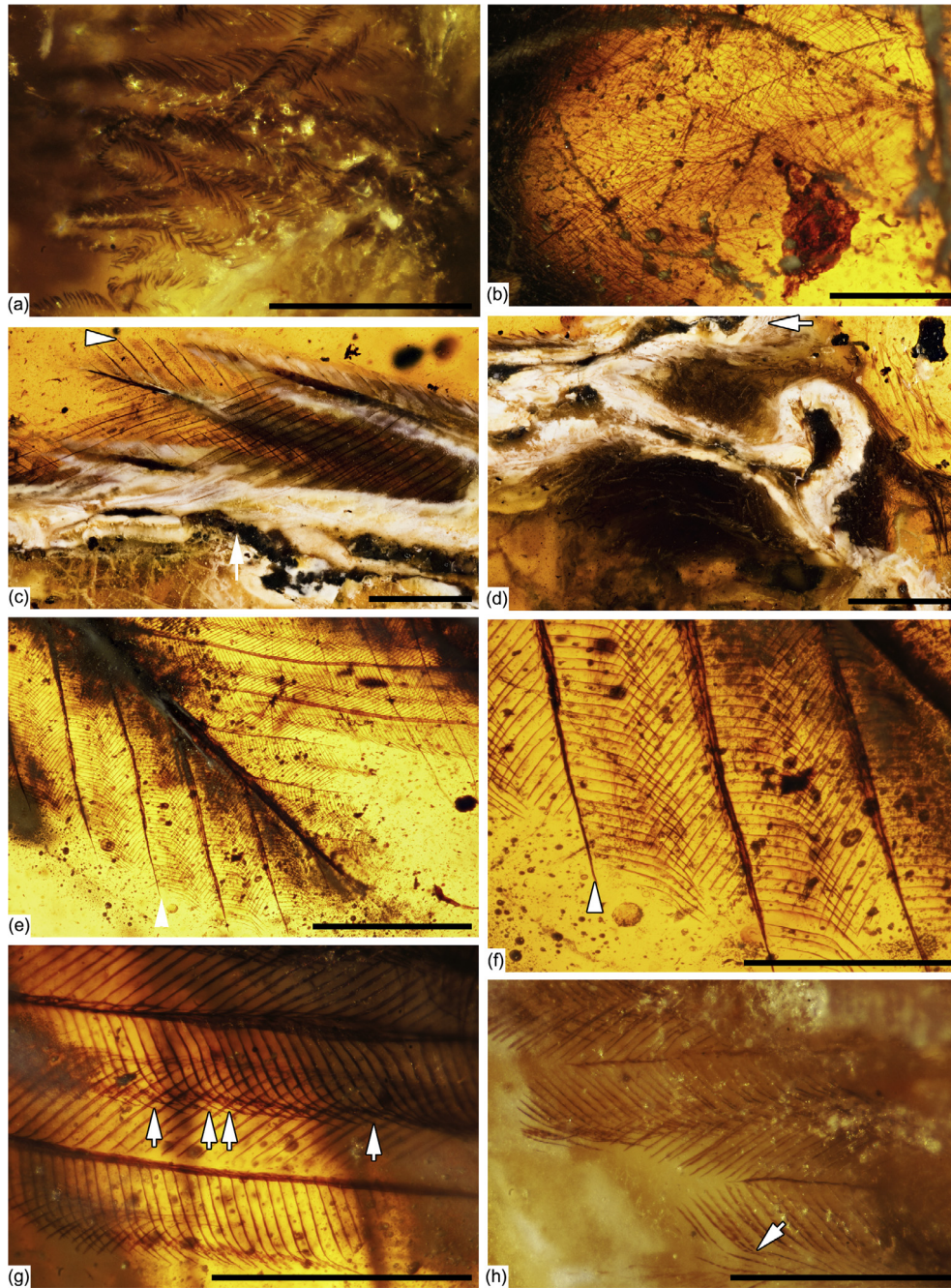


**Fig. 3.** DIP-V-15102 plumage details. (a) Contour feathers from the posterior margin of the head, with pale rami and basal barbules; (b) Detached semiplumes from the breast or neck region; (c) Oblique section through primary feathers that extend through veil of milky amber and away from carbonized tissues of wing (arrow), arrowhead indicates shared point (with e, f); (d) Cross-sectional view of leading edge of wing (arrow, also in Fig. 2f), with underwing coverts and convoluted flap of skin from propropatagium; (e, f) Primary feather cut obliquely to reveal deep rachis and rami, and asymmetrical, widely spaced barbules; (g) Hooklets on primary feather barbules (arrows); (h) Primary covert feathers with well-developed flagellum (inclined arrow). Scale bars equal 0.5 mm (a, b, f–h); 2 mm (c, d); 1 mm (e).

it is exposed at the surface of the amber. Subdomains 2 and 3 are situated over the inclusion, but the body is overlain by a significant thickness of amber in these regions. Subdomain 3 is buried more deeply than subdomain 2. Subdomain 4 measures amber that does not overlie the avialan inclusion.

Eleven elements can be observed through the analysis of  $\mu$ -XFI data, and they are Fe, Ca, Ti, Zn, As, Mn, Br, Cu, Ga, Ni, and K. These elements are listed in the order of relative abundance, from high to low, in Table 1. The elemental abundances are generally propor-

tional to the X-ray fluorescence intensity. The X-ray fluorescence intensity of Fe is two orders of magnitude higher than that of other elements.

In the distribution maps of Fe, Ca, Ti, Zn, As, and Mn these six elements are obviously correlated with the shape of subdomain 1, meaning that the six elements are components of the inclusion itself. The distributions of Ca and Ti (and to a lesser extent, Mn) are relatively concentrated near the boundary of subdomain 1, appearing as a series of thin blue lines and 'hot spots' in the

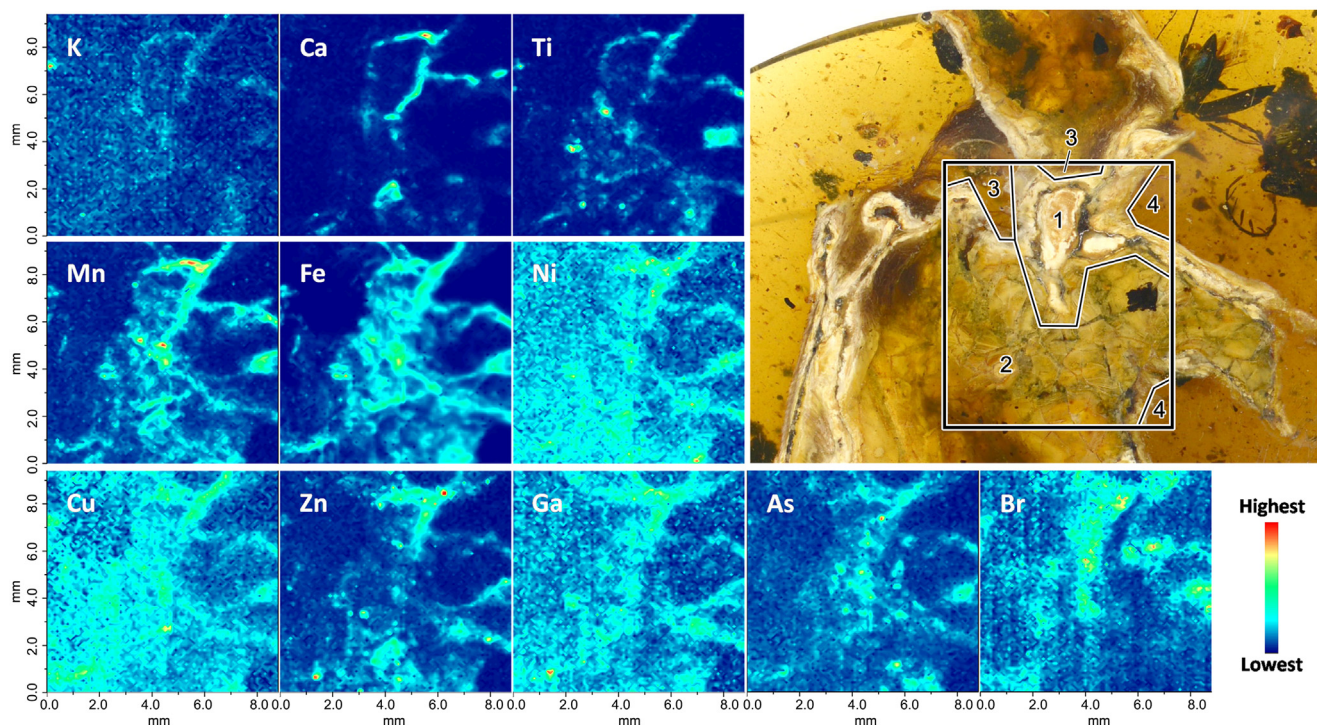


**Fig. 4.**  $\mu$ -XFI elemental maps from DIP-V-15102 head and neck exposures. Photographic inset outlines area for each elemental map, and individual sampling domains are described in the main text. ‘Warmer’ colors in each elemental map indicate higher relative abundance.

**Table 1**

Relative X-ray fluorescence intensity of the elements in Fig. 4.

Element	Fe	Zn	Cu	Mn	Ca	Br	Kr
Relative intensity	100	0.87	0.61	0.6	0.55	0.46	0.39
Element	Ti	As	Ni	Ga	Ge	V	Cr
Relative intensity	0.36	0.34	0.19	0.11	0.09	0.06	0.04

distribution map. The cervical vertebra centrum exposed at the center of subdomain 1 does not have a strong signal for Ca across its entire width—this appears to be a result of pneumatic or highly porous bone. The highest concentrations of elements such as Fe and Mn largely parallel the areas where carbon films (the remains of soft tissues) are exposed at the surface of the amber sample, or exposed by cracks within the veil of milky amber that cover most of the buried body regions. The other 4 elements, Cu, Ga, Ni and K, have relatively high abundances in subdomain 1 and its boundary, but are also distributed in subdomain 2 and 3. Regions containing plumage (subdomain 3) do not display heightened levels of Cu that could be attributable to pigments within the plumage. There is also no obvious correlation between the distribution map of Br and the shape of subdomain 1.

#### 4. Discussion

Osteological characters preserved in DIP-V-15102 suggest the specimen is referable to the Enantiornithes, as are all other birds found in Burmese amber thus far. There are no unequivocal autapomorphies of the Enantiornithes preserved, however the

combination of observed features (e.g., wide U-shaped pubis, cranio-caudally compressed distal humerus) supports this as the most likely identification, further supported by size (very small), and plumage (similar to other enantiornithines and indicative of a precocial juvenile).

Although there are no taphonomic indicators within the amber piece to suggest whether the animal first contacted the resin while alive or dead, indicators exist for much of the subsequent preservation process. The ventral side of the body was facing upward during entombment, and much of the ventral surface was removed through processes such as weathering or scavenging. The corpse is surrounded insect frass and plant fragments, suggesting that the amber piece may have formed on or near the forest floor [23]. Syninclusions such as the large cockroach (Blattodea [24]) situated near the right femur may have been involved in the scavenging process for the exposed corpse [25]. Some of the dinosaur remains reported from Burmese amber have been accompanied by inclusions of either cockroaches or ants (Formicidae: Sphecomyrminae [26]) (e.g., [5]). However, these groups of insects are thought to be predators or generalist feeders that originated before the Cretaceous [27,28]: a much larger sample size is required to support any conclusions about scavenging. If these associations

are recovered repeatedly, they may provide insight into which groups of insects were acting as scavengers for larger corpses in Cretaceous forests.

Chemical mapping of the exposed surface indicates that under the veil of milky amber that surrounds the bird, traces of original material or decay products [29] are preserved in their original positions. The correspondence between XFI maps of iron concentrations and the carbon films left behind by soft tissues or their decay products, as well as calcium with the positions of exposed bones, indicates that very little exchange or replacement has occurred. Despite the lack of preserved internal organs and the high degree of compaction found in DIP-V-15102, many of the bones are still translucent and retain traces of microstructure. The specimen appears to have been largely isolated from surface interactions once it was fully encapsulated by resin flows.

DIP-V-15102 exhibits plumage that is consistent with other fragmentary members of Enantiornithes recovered from Burmese amber, but there are no diagnostic characters among the feathers. The greater density and length of the feathers preserved along the exposed neck and head regions may suggest that this individual had progressed further in its development than the hatchling [6] or juvenile remains [4] reported from the deposit. However, distortion of the bones does not permit observations of sutures or growth plates that would provide independent support for this developmental suggestion based on X-ray  $\mu$ CT data: the small size of the specimen also suggests a juvenile though. (DIP-V-15102 measures approximately 6.2 cm from the base of the skull to the posterior margin of the pubis; while HPG-15-1, a hatchling thought to be within the first week of life, is approximately 4.1 cm long from the base of the skull to the tip of the tail, with a high degree of curvature.) The exposed primary feathers exhibit narrow and deep rachises and barb rami, as well as closed-vane structures and microstructures, indicating rigid feathers capable of flight. The visible portions of each primary are not sufficient to assess flight capability based on barb asymmetry within each vane [30]. The barb divergence angles from the rachis ( $\sim 32^\circ$  leading,  $\sim 40^\circ$  trailing barbs) are more consistent with feathers from advanced flying birds than to taxa basal to Enantiornithes [31].

## 5. Conclusions

Decay and interactions with the surrounding resin have obscured many of the features of DIP-V-15102, but X-ray  $\mu$ CT is able to provide some osteological information, and the coronal section yields an interesting picture of preservation. The balance of osteological evidence preserved in DIP-V-15102 points towards a source within Enantiornithes. The plumage preserved is also consistent with this placement. The remains are compacted into an amber thickness of approximately 7 mm, but they provide a better sense of how a relatively complete and moist corpse behaves upon entering this preservational setting. Hopefully, this specimen provides a better search image for future discoveries, improving recovery rates and reducing losses due to specimen preparation.

## Acknowledgments

We thank Xing Xu for constructive comments on an early version of this paper. This work was funded by the National Natural Science Foundation of China (41790455, 41772008, 31672345, Special Subjects in Animal Taxonomy, NSFC-J1210002); Natural Sciences and Engineering Research Council of Canada (2015-00681); Scientific Research Equipment Development Project of

Chinese Academy of Sciences (YZ201509); and the National Geographic Society, USA (EC0768-15).

## Author contributions

Xing L, O'Connor JK, McKellar RC, Li G designed the project, Xing L, O'Connor JK, McKellar RC, Chiappe L, Bai M, Tseng K, Zhang J, Yang H, Fang J, and Li G performed the research, and Xing L, O'Connor J, McKellar R, Chiappe L, and Li G. wrote the manuscript.

## Conflict of interest

The authors declare that they have no conflict of interest.

## Appendix A. Supplementary data

Supplementary data associated with this article can be found, in the online version, at <https://doi.org/10.1016/j.scib.2018.01.019>.

## References

- [1] Grimaldi DA, Engel MS, Nascimbene PC. Fossiliferous Cretaceous amber from Myanmar (Burma): its rediscovery, biotic diversity, and paleontological significance. *Am Mus Novit* 2002;3361:1–72.
- [2] Ross A, Mellish C, York P, et al. Burmese amber. In: Penney D, editor. *Biodiversity of fossils in amber from the major world deposits*. Manchester: Siri Sci. Press; 2010. p. 208–35.
- [3] Ross AJ. Burmese (Myanmar) amber taxa, on-line checklist v.2017.2. 73pp. Available from: <http://www.nms.ac.uk/explore/stories/natural-world/burmese-amber/August 9, 2017>.
- [4] Xing L, McKellar RC, Wang M, et al. Mummified precocial bird wings in mid-Cretaceous Burmese amber. *Nat Commun* 2016;7:12089.
- [5] Xing L, McKellar RC, Xu X, et al. A feathered dinosaur tail with primitive plumage trapped in mid-Cretaceous amber. *Curr Biol* 2016;26:3352–60.
- [6] Xing L, O'Connor JK, McKellar RC, et al. A mid-Cretaceous enantiornithine (Aves) hatchling preserved in Burmese amber with unusual plumage. *Gondwana Res* 2017;49:264–77.
- [7] Martínez-Delclòs X, Briggs DE, Peñalver E. Taphonomy of insects in carbonates and amber. *Palaeogeogr Palaeoclim Palaeoecol* 2004;203:19–64.
- [8] Schweitzer MH, Jackson FD, Chiappe LM, et al. Late Cretaceous avian eggs with embryos from Argentina. *J Vert Paleontol* 2002;22:191–5.
- [9] de Souza Carvalho I, Novas FE, Agnolin FL, et al. A Mesozoic bird from Gondwana preserving feathers. *Nat Commun* 2015;6:1–5.
- [10] Zhou Z, Zhang F. A precocial avian embryo from the lower cretaceous of China. *Science* 2004;306:653.
- [11] Chiappe LM, Ji S, Ji Q. Juvenile birds from the early cretaceous of China: implications for enantiornithine ontogeny. *Am Mus Novit* 2007;3594:1–49.
- [12] Zhang F, Zhou Z, Hou L, et al. Early diversification of birds: evidence from a new opposite bird. *Chin Sci Bull* 2001;46:945–9.
- [13] Elzanowski A. Embryonic bird skeletons from the Late Cretaceous of Mongolia. *Palaeontol Pol* 1981;42:147–79.
- [14] Sanz JL, Chiappe LM, Pérez-Moreno B, et al. A nestling bird from the Lower Cretaceous of Spain: implications for avian skull and neck evolution. *Science* 1997;276:1543–6.
- [15] Sanz JL, Chiappe LM, Fernández-Jalvo Y, et al. Palaeontology: an Early Cretaceous pellet. *Nature* 2001;409:998–1000.
- [16] Martin LD, Bonner O. An immature specimen of *Baptornis advenus* from the Cretaceous of Kansas. *Auk* 1977;94:787–9.
- [17] Wogelius RA, Manning PL, Barden HE, et al. Trace metals as biomarkers for eumelanin pigment in the fossil record. *Science* 2011;333:1622–6.
- [18] Vinther J. A guide to the field of palaeo colour. *BioEssays* 2015;37:643–56.
- [19] Solé VA, Papillon E, Cotte M, et al. A multiplatform code for the analysis of energy-dispersive X-ray fluorescence spectra. *Spectrochim Acta B* 2007;62:63–8.
- [20] Lucas AM, Stettenheim PR. *Avian Anatomy: Integument*. Washington: US Gov Print Office; 1972.
- [21] Dove CJ. A descriptive and phylogenetic analysis of plumulaceous feather characters in Charadriiformes. *Ornithol Monogr* 2000;51:1–163.
- [22] Grimaldi DA, Engel MS. *Evolution of the Insects*. Camb Univ Press; 2005.
- [23] Perrichot V. Early Cretaceous amber from south-western France: insight into the Mesozoic litter fauna. *Geol Acta* 2004;2:9–22.
- [24] Brunner von Wattenwyl C. *Nouveau Système des Blattaires*. C. Braumüller; 1865.
- [25] Cornaby BW. Carrion reduction by animals in contrasting tropical habitats. *Biotropica* 2007;6:51–63.
- [26] Wilson EO, Carpenter FM, Brown Jr WL. The first Mesozoic ants, with the description of a new subfamily. *Psyche* 1967;74:1–19.
- [27] Barden P, Grimaldi DA. Adaptive radiation in socially advanced stem-group ants from the Cretaceous. *Curr Biol* 2016;26:515–21.

- [28] Wang Z, Shi Y, Qiu Z, et al. Reconstructing the phylogeny of Blattodea: robust support for interfamilial relationships and major clades. *Sci Rep* 2018;7:3903.
- [29] Schweitzer MH, Zheng W, Cleland TP, et al. A role for iron and oxygen chemistry in preserving soft tissues, cells and molecules from deep time. *Proc Biol Sci* 2013;281:20132741.
- [30] Wang X, Nudds RL, Palmer C, et al. Primary feather vane asymmetry should not be used to predict the flight capabilities of feathered fossils. *Sci Bull* 2017;62:1227–8.
- [31] Feo TJ, Field DJ, Prum RO. Barb geometry of asymmetrical feathers reveals a transitional morphology in the evolution of avian flight. *Proc R Soc Lond B Biol Sci* 2015;282:20142864.